Seismic anisotropy accrued by seven unusually deep local earthquakes (between 50 and 60km) in the Albertine rift: Implications of asthenospheric melt upwelling

Arthur Godfrey Batte (abatte@cns.mak.ac.ug)
Makerere University https://orcid.org/0000-0001-9512-509X

A. Schumann
Goethe-Universitat Frankfurt am Main

E. Twesigomwe
Kabale University

Research article

Keywords: Deep local earthquakes, Seismic anisotropy, Lattice Preferred Orientation, Shape Preferred Orientation, Albertine rift, Rwenzori region

Posted Date: May 20th, 2020

DOI: https://doi.org/10.21203/rs.3.rs-29495/v1

Version of Record: A version of this preprint was published on April 16th, 2021. See the published version at https://doi.org/10.1007/s10950-021-10007-2.

Abstract

We investigated the primary mechanisms triggering the S-wave splitting of 7 unusually deep local earthquakes (between 50km and 60km) that originated in the lithosphere beneath the Rwenzori region, in attempt to develop an understanding of the relationship between anisotropic structures in the lithosphere and tectonic deformation processes. A total of 12 of 44 waveforms showed evidence of SWS on their polarization diagrams and were available for further analysis. The fast-wave direction (φ) and delay-time (δt) were estimated using the covariance matrix and the cross-correlation coefficient methods respectively. We observed a clockwise rotation of NW-SE and ~ENE-WSW trending φ-directions at stations deployed on the southward propagating Lake Albert rift segment. We related these directions to anisotropic fabric, probably lattice preferred orientation of preexisting olivine's a-axis aligned with ESE absolute plate motion (APM) vector. At stations deployed away from the rift valley, we similarly observed WNW-ESE and NNW-SSE patterns of φ-directions which we associated to the shape preferred orientation of structures that were probably frozen in the lithosphere and are aligned with the present-day APM direction. We observed δt values ranging between 0.04±0.01s and 0.43±0.02s that significantly decrease with distance away from the rift axis which further supports the view that the anisotropy observed at stations deployed on the ESE propagating plate is related to aligned melt inclusions frozen into the surrounding lithosphere. We further observe that the δt increases linearly with ray-path length which could probably suggest a fairly uniform anisotropy between 50km to 60km depth.

1. Introduction

1.1. Background

Studies of seismic anisotropy within the mantle have led to advancements in constraining upper mantle deformation by resolving directional features, which may provide information on structures within the upper mantle (Gao et al., 2010). Understanding the structure of the upper mantle, the way it deforms and flows has been attributed to the quantity and quality of seismic data that have been recorded during seismic studies conducted around the world. One common indicator of seismic anisotropy is the strain-induced lattice preferred orientation (LPO) of olivine crystals, whereby a-axes of olivine tend to align parallel with the direction of maximum shear (e.g. Liu et al., 2008). Mantle melting has also been observed to influence seismic anisotropy in magma-producing regions (e.g. Gashawbeza et al., 2004). Alignment of melt-filled pockets can induce seismic anisotropy that does not depend on LPO (e.g. Long and van der Hilst, 2006). Studies of Walker et al. (2004) across the NW-SE striking Anza Graben in Kenya have reported the presence of channels in the base of the lithosphere, which in their opinion could have provided guides to plume related flows. They concluded that partially molten inclusions like dikes can penetrate the lithosphere if there is a steady-state active source of partial melt in the asthenospheric mantle. These dikes can trigger S-wave splitting (SWS) due to the large velocity contrast between magma and surrounding rocks resulting into considerable delay-times (δt). Bagley and Nyblade (2013) similarly observed that seismic anisotropy in East Africa is strongly influenced by magmatic flow in the lower mantle which could suggest a link between the processes in the lower mantle and the tectonic

deformation of the Earth's surface. In the Western rift of the East African rift system (EARS), Tepp et al. (2018) observed rift-parallel fast-wave directions (φ). They argued that the spatial variations in their splitting results from those of earlier studies within the western rift could suggest that the nature of mantle flow is a result of a deflection caused by the presence of deeply rooted cratons. Elsewhere in the EARS, Ayele et al. (2004), observed that the anisotropy in the northern Ethiopian rift is an indication of the alignment of the a-axes of olivine in the asthenosphere with the ridge axis due to material flowing laterally to fill the gap that was developed during the lithospheric extension.

This paper reviews the research conducted on a cluster of 7 unusually deep local earthquakes that originated at extraordinary depths (between 50 and 60 km) beneath the Rwenzori region. These earthquakes were recorded between 2nd and 16th September, 2006 at 12 seismic stations setup in the Rwenzori region of the Albertine rift (see Lindenfeld and Rümpker, 2011) during the RiftLink research project [www.riftlink.org]. The Albertine rift, a roughly NE to ENE trending sector of the EARS, extends along the western boundary of Uganda and the neighbouring Democratic Republic of Congo (DRC). Within the Albertine rift are the 5000 m high Rwenzori block mountains. Studies by Koehn et al. (2008) have shown that the Rwenzori block mountains were captured by two rift segments, the Albertine rift segment that extends west of the mountains from Lake Edward in the south to Lake Albert in the north, and the Lake George rift segment that extends east of the mountains from Lake Edward terminating north of Lake George (Shown by a gray arrows in Fig. 2b). In this study, we focus attention on investigating the primary mechanism triggering the SWS of these deep local earthquakes in attempt to developing an understanding of the relationship between anisotropic structures within the upper mantle and tectonic deformation processes beneath the Rwenzori region.

1.2. How reliable are these earthquakes?

Lindenfeld and Rümpker (2011) located these 7 deep local earthquakes using the HYPOCENTER location algorithm of Lienert and Havskov (1995). To evaluate the reliability of the location algorithm, they re-located the hypocenters using both the IASP91 velocity model of Kennett and Engdahl (1991) and the double-difference algorithm (hypoDD) of Waldhauser and Ellsworth (2000). They concluded that in all cases, there were no significant deviations in the depth distributions and that the event locations were reliable with a precision better than 5 km. Therefore, the depths observed for these 7 deep local events are robust and cannot be related to artefacts that could have been caused by cycle-skipping on the waveforms.

Wölbern et al. (2010) used observations derived from teleseismic receiver functions to constrain the thickness of the crust beneath the Rwenzori region. Using the method of Zhu and Kanamori (2000), they observed a crustal thickness of about 30 km on the eastern rift flank, 20 km and 28 km beneath the northern and central parts of the Rwenzori block. It is therefore unlikely for these deep local earthquakes to have originated from the crust, but rather in the lithospheric mantle beneath the Rwenzori region. It was initially not clear how these deep local earthquakes could have originated from such an unexpected depth. Schmeling and Wallner (2012) associated these deep focus earthquakes to the rift induced delamination process beneath the Rwenzori block. However, their findings were inconclusive. Lindenfeld

and Rümpker (2011) therefore argued that these deep earthquakes did not originate directly below the Rwenzori block and that magmatic impregnation of the mantle lithosphere described by Foley (2008) could be a likely cause of seismic radiation at such an unexpected depth.

2. Material And Methods

We used data that were recorded by EDL and REFTEK data loggers, coupled with a Güralp CMG-3T and Mark L-4C3D seismometers respectively, operating in continuous and trigger modes respectively and sampling at 100 samples/second. We applied the Short-term and Long-term Average (STA, LTA) to the continuous data streams to detect and extract local events. We used a STA and LTA of 3 s and 30 s respectively for the time windows and a STA/LTA ratio of 3.0 as a trigger to an event. We adopted a critical angle for the S-wave window of $\leq 34°$, which according to Booth and Crampin (1985) is adequate for minimizing contaminations from S- to P-wave mode conversions near the surface. Booth and Crampin (1985) further observed that these contaminations distort the amplitude and phase of the recorded wave and consequently yielding a nonlinear particle motion.

The 7 deep local earthquakes that were recorded at 12 seismic stations yielded 44 waveforms for SWS analyses (Table 1). The horizontal waveforms were initially butterworth filtered between 0.1 and 10 Hz to separate the dominant frequency from the noise. In this study, we applied both the automatic and visual display techniques to estimate the splitting parameters. It suffices to say that each has its advantages and drawbacks however, the most optimal approach is combining the advantages of both display (polarization diagrams and rotated seismograms) and automatic (cross correlation and covariance techniques) techniques for measuring the splitting parameters (Gao et al., 2006). We implemented the particle motion analysis of (Crampin et al., 1985) to estimate the SWS parameters. We used only the traces that showed abrupt changes in φ-directions on their polarization diagrams (Fig. 1b). Only 12 waveforms showed evidence of abrupt changes in φ-direction (with dashes in Table 1). The rest of the traces were rejected due to either due to low signal-to-noise ratio or lack of anisotropic evidences.

Because we analyzed horizontal seismograms for SWS, we only resolved the horizontal projection of φ-direction, therefore, the waveforms that showed a cruciform particle motion were rotated into the fast and slow coordinate system (Fig. 1c). For each measurement, we selected a time window that included the earliest S-wave arrival and φ-direction in the horizontal plane was estimated using the covariance matrix method. This method was initially incited basing on the theory of polarization filters.

Shimshoni and Smith (1964) used this method to constrain the rectilinearity on recorded seismograms. Since then, a number of researchers have used this theory to develop applications that detect phase arrivals on seismograms (e.g. Montalbetti and Kanasewich, 1970). The covariance matrix method uses the covariance matrix (*CM*) of the horizontal channels (*N, E*) for ‘n’ set of points taken from within a specific time window to estimate the φ-direction.

$$CM = \begin{bmatrix} var_N & cov_{NE} \\ cov_{NE} & var_E \end{bmatrix}$$

We diagnosed the covariance matrix and estimated the φ-direction considering the eigenvector associated with the largest eigenvalue with respect to the coordinate directions N and E. Given that λ_1 and λ_2 are the largest and next largest eigenvalues of covariance matrix respectively, the function $f(\lambda_1, \lambda_2)$ will tend to unity when rectilinearity is high ($\lambda_1 \gg \lambda_2$) or it will tend to almost zero when rectilinearity is low (when the two principle axes approach one another in magnitude).

$$f(\lambda_1, \lambda_2) = 1 - \left[\frac{\lambda_2}{\lambda_1}\right]^n$$

The polarized fast and slow traces will split in time when they come across an anisotropic media and the two S-waves will appear as identical wavelets separated by a certain δt. In an isotropic environment however, the split is preserved along the ray path (Díaz et al., 2006). We estimated the δt between the fast and slow horizontal channels using the cross-correlation coefficient method (Fig. 1d).

This method was initially implemented by (Fukao, 1984). The cross-correlation technique has been successively implemented in most automatic measurement techniques to estimate the δt both above small earthquakes in the crust, and in upper mantle anisotropy. This technique estimates the δt from lags of cross-correlations of the preferentially rotated wave-trains. It is however imperative to evaluate the quality of φ and δt in order to ensure reliability of the splitting measurements. We therefore adopted the standard error of the mean technique, which is a standard statistical approach to access the uncertainties in the splitting parameters at a 95% confidence level.

Station	Equipment	Seismic event	slon [^{o}]	slat [^{o}]	hypo-dist [km]	φ [^{o}]	δt [s]
KMTW	a	060916202630.KMTW	30.384	0.7425	59.9	-	-
BUTU	c	060902021330.BUTU	30.168	0.5620	64.5	168±10.0	0.43±0.018
BUMA	c	060902021330.BUMA	30.066	0.6943	67.5	81±6.8	0.28±0.017
KABA	b	060902021330.KABA	30.132	0.7753	63.9	78±2.81	0.25±0.019
		060903231040.KABA			63.6	-	–
		060904025550.KABA			61.8	-	-
		060914115320.KABA			64.4	-	-
		060914133540.KABA			65.6	-	-
		060916202630.KABA			68.7	140±0.65	0.24±0.016
KABG	a	060902021330.KABG	30.649	0.6308	63.3	-	-
		060903231040.KABG			64.1	-	-
		060904025550.KABG			60.5	-	-
		060914133540.KABG			63.8	-	-
		060916202630.KABG			65.7	-	-
		060916203940.KABG			63.4	-	-
KAGO	b	060914133540.KAGO	30.461	0.6823	57.7	-	-
		060916202630.KAGO			60.4	-	-
		060916203940.KAGO			57.8	-	-
KASS	b	060902021330.KASS	30.309	0.5682	59.6	110±2.06	0.21±0.014
		060904025550.KASS			57.8	-	-
		060914115320.KASS			60.8	115±1.87	0.24±0.015
		060914133540.KASS			62.0	-	-
		060916202630.KASS			65.3	-	-
KISA	b	060916202630.KISA	30.743	0.5937	71.1		
KYAM	c	060902021330.KYAM	30.276	0.6858	58.0		
MIRA	b	060902021330.MIRA	30.569	0.6585	59.5	77±1.43	0.04±0.018
		060903231040.MIRA			60.1	104±2.17	0.05±0.012
		060904025550.MIRA			56.6	-	-
		060914115320.MIRA			59.2	-	-
		060914133540.MIRA			60.2	-	-
		060916202630.MIRA			62.4	-	-
		060916203940.MIRA			59.9	143±11.9	0.05±0.011
NTAN	c	060902021330.NTAN	30.151	0.8038	63.3	95±1.43	0.22±0.014
		060904025550.NTAN			61.0	-	-
		060914115320.NTAN			63.5	-	-
		060914133540.NTAN			64.8	130±0.5	0.37±0.019
		060916202630.NTAN			67.7	125±1.14	0.35±0.021
SEMP	b	060902021330.SEMP	30.168	0.8350	63.1	-	-
		060903231040.SEMP			62.0	-	-
		060904025550.SEMP			60.6	-	-
		060914115340.SEMP			63.2	-	-
		060914133540.SEMP			64.3	-	-
		060916202630.SEMP			67.2	-	-
		060916203940.SEMP			64.3	-	-

Table 1. Showing 44 waveforms recorded at the twelve (12) seismic stations. The data logger/seismometer are given as a, b and c corresponding to EDL PR6-24/Guralp GMG-3T, EDL PR6-24/Mark L-4C3D and REFTEK 72A-07/Mark L-4C3D respectively. hypo-dist corresponds to the hypocenter distance. The dashes imply no measurement were estimated due to low signal-to-noise ratios and/or lack of anisotropic evidence. The coordinates slon and slat are seismic station longitudes and latitudes respectively.

3. Results

We report our splitting measurements as thick black lines that are scaled by δt and aligned by φ (Fig. 2a). The red cones in the background of each measurement represent the uncertainties in the splitting results at 95% confidence level. To avoid cluttering of the measurements at a station, we plot our splitting parameters in the vicinity of the seismic station at arbitrary locations, specifically those where more than one measurement were analyzed. In order to associate the splitting result with its corresponding earthquake, we plot the corresponding earthquake in the middle of each measurement.

We partitioned the region into two sub regions i.e. those on the southward propagating rift segment (Fig. 2b: red ellipse) and those on the propagating Victoria plate (Fig. 2b: blue ellipse). Figure 2a was quite revealing in several ways. First, we observed a clockwise rotation of φ-directions from NW-SE and ~ ENE-WSW at stations on the southward propagating rift segment (BUMA, KABA and NTAN). Second, at stations deployed on the Victoria plate (BUTU, KASS and MIRA) however, we similarly observed WNW-ESE and NNW-SSE orientation patterns of φ-directions which tend to align with the ESE APM vector (Fig. 2a).

In fact, the φ-directions in our study area are consistent with the asthenospheric mantle flow model of Sleep et al. (2002). It should be mentioned that the Victoria microplate is part of the old Congo-Tanzanian Craton (Calais et al. 2006) which according to Koehn et al. (2010) is still connected to the northern tip of the Rwenzori Mountains, an extraordinary basement block that developed within the western branch of the EARS. Table 1 shows the station-earthquake pairs with δt values ranging between 0.04 ± 0.02 s and 0.43 ± 0.02 s. Figure 3a shows that the magnitude of splitting measurements vary across the rift. The largest δt values were observed along the edges of the fault-bounded rift valley, which decay away from the NNE-trending rift axis (the blue dotted lines in Fig. 2a).

4. Discussion

Issues regarding the relationship between strain and anisotropy have been a controversial and much disputed subject within the field of seismology (e.g. Savage, 1999). To commence our discussion, we initially examine the kinematics and magnitude of active and past deformation mechanisms manifesting in the lithosphere beneath the Rwenzori region and attempt to associate them with the observed anisotropy in the region. It seems likely that both aligned melt intrusion zones within the lithosphere and aligned asthenospheric flow mechanisms for anisotropy are at play in our study region. Factors that are thought to be influencing seismic anisotropy in the mantle have been explored in several studies. For example, Karato and Jung (2003) have associated seismic anisotropy in the mantle to the alignment of the *a*-axis of olivine through dislocation creep. Numerical models of Tommasi et al. (1999) similarly draws our attention to the LPO of pre-existing olivine to be reactivated in a direction that combines both strike-slip motion and extension regimes, parallel and orthogonal to the rift axis respectively. With all factors typical in their opinion, they added that this deformation regime would consequently invoke a composite LPO of preexisting *a*-axis of olivine, oblique to the orientation of the rift axis. Similar inferences have been made to support this oblique deformation by (e.g. Rümpker et al., 2003). Numerous

studies have attempted to explain the nature of olivine. A study by Walker et al. (2004) reports that olivine comprises a significant fraction of the upper mantle and when deformed via dislocation creep, one or more of the three olivine crystallographic axes develop LPO, an indication of anisotropy. Gao et al. (1997) in their study argue that the φ-directions in the asthenospheric mantle are related to LPO of olivine's *a*-axis that is aligned with the present-day APM vector which according to Vinnik et al. (1992) can be related to asthenospheric shear. Studies by Stamps et al. (2008) have shown that the Albertine rift is currently opening at a velocity of 2.1 mm/yr and that the Victoria microplate on the eastern side of the Rwenzori block is propagating in an ESE direction relative to the Nubia plate on the western side. An ESE propagating direction of the Victoria microplate at a velocity of about 5 mm/yr has been suggested by Calais et al. (2006). Interestingly, our results of φ-directions at stations in the rift are consistent with the present-day rift-perpendicular ESE APM vector, which is not surprising given the long history of extension in the region.

We initially seek to address two questions: (1) is it possible that dynamic stretching of the lithosphere occurred beneath the Rwenzori region that could have resulted into a lithospheric thickness of < 50 km (especially in the rift valley), and that this thinning was compensated for by balancing the ascent of asthenospheric melt along the inverted valleys that follow the convex-like base of the lithosphere? (2) if the lithospheric thinning was not sufficient enough, is it possible that the asthenospheric melt extruded into a thick lithosphere to shallow depths of < 50km? If any of these hypotheses is correct and considering the location of these deep earthquakes (which in fact are located slightly away from the rift valley; see Fig. 2a), then it is likely that the travel-path from the earthquakes to the stations deployed on the southward propagating rift segment (BUMA, KABA and NTAN) could have traversed through the upwelled asthenospheric melt triggering olivine-induced SWS assuming olivine LPO. Analyses emanating from the geochemical analysis of volcanic rocks by Link et al. (2010) has reported lithospheric thinning from > 140 km beneath Toro-Ankole (Western Uganda) to about 80 km beneath the Virunga volcanic field in the DRC. Other studies by Wölbern et al. (2012) have placed the thickness of the crust at 30 km, the upper boundary of the lithosphere at 60 km and the lithosphere-asthenosphere boundary at 120 km.

With regards to magmatic upwelling in the Rwenzori region, there have been several reports to confirm the presence of magmatic material beneath our study area. Numerical models of e.g. Wallner and Schmeling (2010) predict upwelling of a broad region of asthenospheric melt into the lithosphere below the Rwenzori block. A study of *b*-values distribution in the Rwenzori region by Batte and Rümpker (2019) has reported the occurrence of broad magmatic chambers beneath the Rwenzori region. Studies of Lindenfeld et al. (2012); Wölbern et al. (2012); Wölbern et al. (2010) similarly offer evidence which suggests the presence of magmatic intrusions into the lithosphere beneath the Rwenzori region. Ochmann et al. (2007) observed temperature anomalies that they associated to a hot degassing magmatic intrusion which the believe could be a possible heat source for the nearby Sempaya hotspring (red star in Fig. 2b). If these concepts are true, then it is likely that an upward penetration of asthenospheric melt into the lithosphere associated with rifting could be the most plausible cause of the observed φ-directions at stations BUMA, NTAN and KABA. The magmatic material formed from decompression melting of the asthenospheric mantle could have intruded the lithosphere and was deflected by the migrating plate leading to the formation of

anisotropic fabrics that are aligned with the APM vector. Studies by Meissner et al. (2006) have shown that magmatic melts from the mantle extruded into the lower crust causing heating and layering. These authors continued to argue that ductile deformation is responsible for the alignment of anisotropic minerals leading to transverse isotropy or azimuthal anisotropy. Similar inferences have been made across the East African Plateau by Walker et al. (2004). It is therefore possible that the almost ENE-WSW patterns of φ-directions observed at BUMA, KABA and NTAN could be related to the alignment of the anisotropic fabric associated with the transcurrent flow of the upwelled asthenospheric melt that was driven by plate migration, possibly during a prior event of rifting. Of course, we cannot rule out the fact that the measurements at stations within the rift show significant scatter. These φ-directions, based on the assumption of a single anisotropic layer reveal a conspicuous change in the φ-direction pattern from almost ENE-WSW to NW-SE direction. This could probably be related to local structural irregularities or a more complex anisotropic symmetry beneath the region. It could also be interpreted as due to the presence of a structure more complex than a single anisotropic layer beneath this area.

We continue to discuss the anisotropy observed at stations deployed away from the rift valley, on the ESE propagating Victoria microplate (KASS, BUTU and MIRA). We could similarly argue that the observed φ-directions at these stations is influenced by LPO of olivine's a-axis that are aligned with the proposed ESE APM vector. However, since the lithosphere is rigid and given that asthenospheric upwelling and magmatism in the lithospheric plate away from the rift is relatively minimal, it is unlikely for this pattern of φ-directions to be associated with olivine's a-axes as we presumed, other than the shape preferred orientation (SPO) of structures that were trapped and frozen in the lithosphere and are aligned parallel to the present-day APM direction of the Victoria plate. Similar inferences have been made by Gao et al. (1997) during their study across the Kenya rift. Factors that are thought to be influencing the SPO of water-filled or melt-filled dikes/lenses within the lithosphere have been explored in several studies (e.g. Walker et al., 2004) which in their opinion can induce effective anisotropy. Studies by Kendall et al. (2005) have shown increased splitting coupled with increased magma production near breakup in the Ethiopian rift. They continue to argue that the melt will solidify, drifting away from the mantle upwelling and consequently, leaving a residual anisotropy predominantly due to crystal alignment. Studies by Foley (1992) have reported highly potassic and silica under-saturated lavas beneath the Rwenzori region, which they related to small-scale veins within the lowermost lithosphere. This according to (e.g. Foley et al., 2012) would indicate a presence of small-scale dikes and melt-filled lenses below the crust between 60 and 140 km.

Pockets/lenses of melt inclusions into the lithosphere can have a significant influence on observed seismic anisotropy. Studies by Walker et al. (2004) have shown the δt values to be large at the center of the rift, but diminish with distance away from the rift which they interpret as being due to the cooling of the dikes/magma lenses over time. A close inspection of our δt values reveals a significant decrease with distance away from the rift axis (Fig. 3a) which further complements our previous conclusion that the observed anisotropy beneath the stations (BUTU, KASS and MIRA) is due to rift structures, probably aligned melt inclusions frozen into the surrounding lithosphere. The NNW-SSW pattern of φ-direction at station BUTU deserves mention. This station was located where the Rwenzori basement block connects

with the Victoria plate. It is possible that this pattern of φ-direction could have resulted from the perturbation of the stress field which according to Koehn et al. (2008) could be a consequence of the southward propagating rift segment. Alternatively, it could have been a result of the clockwise rotation of the Rwenzori block (Koehn et al. 2010) which according to Koehn et al. (2008) could have led to the formation of local compression related structures at corners where the micro-plates are still attached to larger scale plates. We of course cannot rule out the fact that a significant contribution of the observed δt is from crustal sources, since the crust accounts for about 50% of the travel path (20–30 km crustal thickness). Studies of SWS on local earthquakes (focal depth ≤ 30 km) in the crust beneath the Rwenzori region by Batte et al. (2014) have reported an average δt of 0.04 s (~ 4% anisotropy) which they related to the presence of stress aligned pockets of melt within the shallow crust. They observe a heterogeneous pattern of φ-directions which the attribute to the extensive dilatancy anisotropy hypothesis of Crampin and Lovell (1991).

SWS analyses on teleseismic earthquakes recorded in the Rwenzori region have been completed by Homuth et al. (2016). They have reported rift-parallel φ-directions that are consistent with horizontal transverse anisotropy, which is typical during the early stages of continental rifting. They concluded that these φ-directions are related to rift-parallel intrusions or lenses in the lithospheric mantle located at depths between 60 and 120 km. They further observe δt values ranging between 0.2 s and 2.0 s (average ≈ 1.0 s). We however observed an average of ~ 0.23 s (~ 23% anisotropy) that was accrued from deep local sources. It is therefore clear that the major contribution of seismic anisotropy in the Rwenzori region is accrued from teleseismic sources (~ 73% anisotropy). We further observe that the δt increases linearly with ray-path length (Fig. 4) which could suggest a fairly uniform anisotropy between 50 km and 60 km depth. A similar inference was made by Keir et al. (2005) in their study across the Ethiopian rift. Whatever the mechanisms that triggers SWS at such an unexpected depth, if our interpretations are correct may suggest evidence of a profound deformation regime, which may have important implications on the understanding of the geotectonic evolution of the lithospheric mantle beneath Rwenzori region.

5. Conclusions

Studies of SWS beneath the Rwenzori region were completed on 7 unusually deep local earthquakes that originated between 50 and 60 km. Only 44 waveforms were available for interpretation from which, 12 showed abrupt changes in the φ-direction on their polarization diagrams. We observed WNW-ESE and E-W orientation patterns of φ-directions at stations deployed on the southward propagating rift segment (BUMA, KABA and NTAN) which we related to the presence of anisotropic fabrics (probably LPO of olivine), formed as a result of the deflection of the asthenospheric melt that extruded into the lithosphere by the ESE propagating plate, and are aligned with the APM vector. At stations deployed away from the rift valley (BUTU, KASS and MIRA) however, we observed WNW-ESE and NNW-SSE patterns of φ-directions which we associated to the shape preferred orientation of melt-filled pockets trapped in the lithosphere that are aligned with the present-day APM direction. The δt values accrued by these deep events range between 0.04 ± 0.01 s and 0.43 ± 0.02 s. These δt values significantly decrease with distance away from the rift (MIRA being the farthest station from the rift valley) which further supports

our idea that the observed anisotropy beneath the stations (BUTU, KASS and MIRA) is due to rift structures, probably aligned melt inclusions frozen into the surrounding lithosphere. We further observe that the δt increases linearly with ray-path length which could suggest a fairly uniform anisotropy between 50 km to 60 km depth.

Declarations

- **Availability of Dataset**

Supplementary data associated with this article is available in the Makerere University Institutional Repository at http://hdl.handle.net/10570/7597 under the name Earthquake data files. It is License free with no restrictions attached.

- **Competing Interests**

The authors declare that they have no known competing financial interests or personal relationships that could have appeared to influence the work reported in this paper.

- **Funding**

The authors wish to declare the following funding sources:

- The German Research Council (DFG)
- The German Academic Exchange Services (DAAD)

- **Authors' Contribution**

All authors have been intensively involved in the data collection phase, drafting the manuscript and revising it critically for important intellectual content.

- **Acknowledgements**

We the authors strongly acknowledge the financial support offered by the German Research Council for the financial aid they offered towards completion of this research. We also wish to thank the Uganda National Council of Science and Technology, Uganda Wildlife Authority for their unconditional cooperation. We wish to recognize Paul Wessel and Walter, H.F. Smith, authors for the Generic Mapping Tools used.

References

Ayele, A., Stuart, G., and Kendall, J.-M. (2004). Insights into rifting from shear wave splitting and receiver functions: An example from Ethiopia. *Geophys. J. Int., 157*(1), 354-362.

Bagley, B., and Nyblade, A.A. (2013). Seismic anisotropy in eastern Africa, mantle flow, and the African superplume. *Geophys. Res. Lett., 40*(8), 1500-1505.

Batte, A.G., and Rümpker, G. (2019). Spatial mapping of b-value heterogeneity beneath the Rwenzori region, Albertine rift: Evidence of magmatic intrusions. *J. Volcanol. Geoth. Res., 381*, 238-245.

Batte, A.G., Rümpker, G., Lindenfeld, M., and Schumann, A. (2014). Structurally controlled seismic anisotropy above small earthquakes in crustal rocks beneath the Rwenzori region, Albertine Rift, Uganda. *J. Afr. Earth. Sci., 100*, 579-585.

Booth, D.C., and Crampin, S. (1985). Shear-wave polarizations on a curved wavefront at an isotropic free surface. *Geophys. J. Int., 83*(1), 31-45.

Calais, E., Ebinger, C., Hartnady, C., and Nocquet, J. (2006). Kinematics of the East African Rift from GPS and earthquake slip vector data. *Geol. Soc. Lon. Spec. Publ., 259*(1), 9-22.

Crampin, S., Evans, R., and Üçer, S.B. (1985). Analysis of records of local earthquakes: the Turkish Dilatancy Projects (TDP1 and TDP2). *Geophys. J. Int., 83*(1), 1-16.

Crampin, S., Lovell, J.H., 1991. A decade of shear-wave splitting in the Earth's crust: what does it mean? What use can we make of it? And what should we do next? *Geophys. J. Int*. 107, 387-407.

Díaz, J., Gallart, J., Ruiz, M., Pulgar, J., López-Fernández, C., and González-Cortina, J. (2006). Probing seismic anisotropy in North Iberia from shear wave splitting. *Phys. Earth Plan. Int., 158*(2-4), 210-225.

Foley, S.F. (1992). Vein-plus-wall-rock melting mechanisms in the lithosphere and the origin of potassic alkaline magmas. *Lithos, 28*(3-6), 435-453.

Foley, S.F. (2008). Rejuvenation and erosion of the cratonic lithosphere. *Nat. Geosci., 1*(8), 503.

Foley, S.F., Link, K., Tiberindwa, J.V., and Barifaijo, E. (2012). Patterns and origin of igneous activity around the Tanzanian craton. *J. Afr. Earth. Sci., 62*(1), 1-18.

Fukao, Y. (1984). Evidence from core-reflected shear waves for anisotropy in the Earth's mantle. *Nature, 309*(5970), 695.

Gao, S.S., Davis, P.M., Liu, H., Slack, P.D., Rigor, A.W., Zorin, Y.A., Mordvinova, V.V., Kozhevnikov, V.M., and Logatchev, N.A. (1997). SKS splitting beneath continental rift zones. *J. Geophys. Res-Solid, 102*(B10), 22781-22797.

Gao, S.S., Liu, K.H., and Abdelsalam, M.G. (2010). Seismic anisotropy beneath the Afar Depression and adjacent areas: Implications for mantle flow. *J. Geophys. Res-Solid, 115*(B12).

Gao, Y., Hao, P., and Crampin, S. (2006). SWAS: a shear-wave analysis system for semi-automatic measurement of shear-wave splitting above small earthquakes. *Phys. Earth Plan. Int., 159*(1-2), 71-89.

Gashawbeza, E.M., Klemperer, S.L., Nyblade, A.A., Walker, K.T., and Keranen, K.M. (2004). Shear-wave splitting in Ethiopia: Precambrian mantle anisotropy locally modified by Neogene rifting. *Geophys. Res. Lett., 31*(18).

Homuth, B., Löbl, U., Batte, A.G., Link, K., Kasereka, C.M., and Rümpker, G. (2014). Seismic anisotropy of the lithosphere/asthenosphere system beneath the Rwenzori region of the Albertine Rift. *Int. J. Earth Sci*. 105:1681-1692

Karato, S.-I., and Jung, H. (2003). Effects of pressure on high-temperature dislocation creep in olivine. *Philosophical Magazine, 83*(3), 401-414.

Keir, D., Kendall, J.M., Ebinger, C., and Stuart, G. (2005). Variations in late syn-rift melt alignment inferred from shear-wave splitting in crustal earthquakes beneath the Ethiopian rift. *Geophys. Res. Lett., 32*(23).

Kendall, J.-M., Stuart, G., Ebinger, C., Bastow, I., and Keir, D. (2005). Magma-assisted rifting in Ethiopia. *Nature, 433*(7022), 146.

Kennett, B., and Engdahl, E. (1991). Traveltimes for global earthquake location and phase identification. *Geophys. J. Int., 105*(2), 429-465.

Koehn, D., Aanyu, K., Haines, S., and Sachau, T. (2008). Rift nucleation, rift propagation and the creation of basement micro-plates within active rifts. *Tectonophysics, 458*(1-4), 105-116.

Koehn, D., Lindenfeld, M., Rümpker, G., Aanyu, K., Haines, S., Passchier, C., and Sachau, T. (2010). Active transsection faults in rift transfer zones: evidence for complex stress fields and implications for crustal fragmentation processes in the western branch of the East African Rift. *Int. J. Earth. Sci., 99*(7), 1633-1642.

Lienert, B.R., and Havskov, J. (1995). A computer program for locating earthquakes both locally and globally. *Seismol. Res. Lett., 66*(5), 26-36.

Lindenfeld, M., and Rümpker, G. (2011). Detection of mantle earthquakes beneath the East African Rift. *Geophys. J. Int., 186*(1), 1-5.

Lindenfeld, M., Rümpker, G., Link, K., Koehn, D., and Batte, A. (2012). Fluid-triggered earthquake swarms in the Rwenzori region, East African Rift—Evidence for rift initiation. *Tectonophysics, 566*, 95-104.

Link, K., Koehn, D., Barth, M.G., Tiberindwa, J.V., Barifaijo, E., Aanyu, K., and Foley, S.F. (2010). Continuous cratonic crust between the Congo and Tanzania blocks in western Uganda. *Int. J. Earth. Sci., 99*(7), 1559-1573.

Liu, K.H., Gao, S.S., Gao, Y., and Wu, J. (2008). Shear wave splitting and mantle flow associated with the deflected Pacific slab beneath northeast Asia. *J. Geophys. Res-Solid, 113*(B1).

Long, M.D., and van der Hilst, R.D. (2006). Shear wave splitting from local events beneath the Ryukyu arc: Trench-parallel anisotropy in the mantle wedge. *Phys. Earth Plan. Int., 155*(3-4), 300-312.

Meissner, R., Rabbel, W., and Kern, H. (2006). Seismic lamination and anisotropy of the lower continental crust. *Tectonophysics, 416*(1-4), 81-99.

Montalbetti, J.F., and Kanasewich, E.R. (1970). Enhancement of teleseismic body phases with a polarization filter. *Geophys. J. Int., 21*(2), 119-129.

Ochmann, N., Lindenfeld, M., Barbirye, P., and Stadtler, C. (2007). *Microearthquake survey at the Buranga geothermal prospect, western Uganda.* Paper presented at the Proceedings of Thirty-Second Workshop on Geothermal Reservoir Engineering.

Rümpker, G., Ryberg, T., Bock, G., and Group, D.S. (2003). Boundary-layer mantle flow under the Dead Sea transform fault inferred from seismic anisotropy. *Nature, 425*(6957), 497.

Savage, M. (1999). Seismic anisotropy and mantle deformation: what have we learned from shear wave splitting? *Rev. Geophys, 37*(1), 65-106.

Schmeling, H., and Wallner, H. (2012). Magmatic lithospheric heating and weakening during continental rifting: A simple scaling law, a 2-D thermomechanical rifting model and the East African Rift System. *Geochem. Geophys. Geosy., 13*(8).

Shimshoni, M., and Smith, S.W. (1964). Seismic signal enhancement with three-component detectors. *Geophysics, 29*(5), 664-671.

Sleep, N., Ebinger, C., and Kendall, J.-M. (2002). Deflection of mantle plume material by cratonic keels. *Geol. Soc. Lon. Spec. Publ., 199*(1), 135-150.

Stamps, D.S., Calais, E., Saria, E., Hartnady, C., Nocquet, J.M., Ebinger, C.J., and Fernandes, R.M. (2008). A kinematic model for the East African Rift. *Geophys. Res. Lett., 35*(5).

Tepp, G., Ebinger, C., Zal, H., Gallacher, R., Accardo, N., Shillington, D., Gaherty, J., Keir, D., Nyblade, A., and Mbogoni, G. (2018). Seismic anisotropy of the upper mantle below the Western rift, East Africa. *J. Geophys. Res-Solid, 123*(7), 5644-5660.

Tommasi, A., Tikoff, B., and Vauchez, A. (1999). Upper mantle tectonics: three-dimensional deformation, olivine crystallographic fabrics and seismic properties. *Earth Plan. Sci. Lett., 168*(1-2), 173-186.

Vinnik, L., Makeyeva, L., Milev, A., and Usenko, A.Y. (1992). Global patterns of azimuthal anisotropy and deformations in the continental mantle. *Geophys. J. Int., 111*(3), 433-447.

Waldhauser, F., and Ellsworth, W.L. (2000). A double-difference earthquake location algorithm: Method and application to the northern Hayward fault, California. *Bull. Seismol. Soc. Am., 90*(6), 1353-1368.

Walker, K.T., Nyblade, A.A., Klemperer, S.L., Bokelmann, G.H., and Owens, T.J. (2004). On the relationship between extension and anisotropy: Constraints from shear wave splitting across the East African Plateau. *J. Geophys. Res-Solid, 109*(B8).

Wallner, H., and Schmeling, H. (2010). Rift induced delamination of mantle lithosphere and crustal uplift: a new mechanism for explaining Rwenzori Mountains' extreme elevation? *Int. J. Earth. Sci., 99*(7), 1511-1524.

Wölbern, I., Rümpker, G., Link, K., and Sodoudi, F. (2012). Melt infiltration of the lower lithosphere beneath the Tanzania craton and the Albertine rift inferred from S receiver functions. *Geochem. Geophys. Geosy., 13*(8).

Wölbern, I., Rümpker, G., Schumann, A., and Muwanga, A. (2010). Crustal thinning beneath the Rwenzori region, Albertine rift, Uganda, from receiver-function analysis. *Int. J. Earth. Sci., 99*(7), 1545-1557.

Zhu, L., and Kanamori, H. (2000). Moho depth variation in southern California from teleseismic receiver functions. *J. Geophys. Res-Solid, 105*(B2), 2969-2980.

Figures

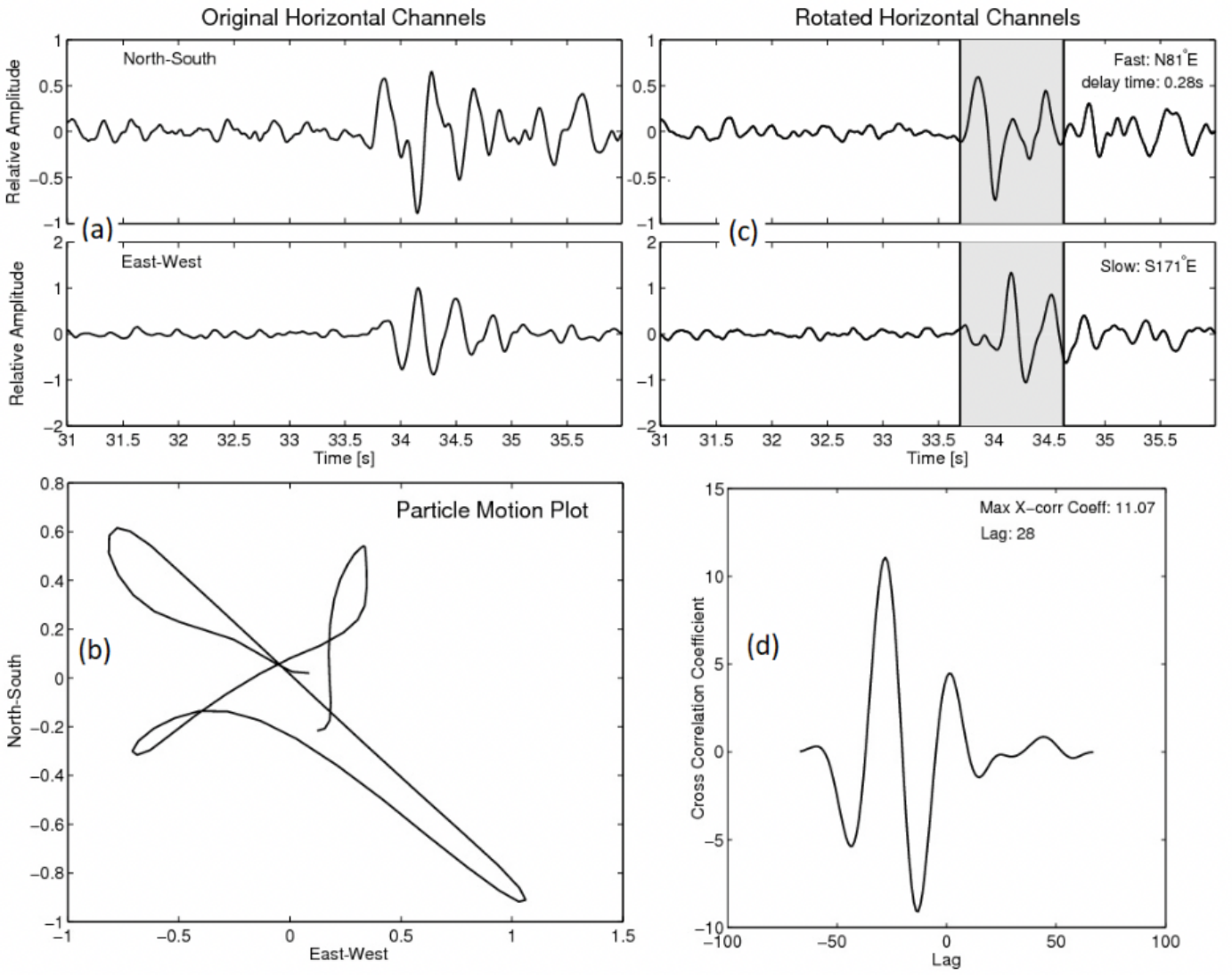

Figure 1

Example of SWS of a seismic waveform. (a) original waveforms in the horizontal coordinate system, (b) cruciform particle motion showing evidence of SWS, and (c) the rotated waveforms (into fast and slow horizontal channels). The time window (vertical grey shading) shows difference between the onsets of the fast and slow shear waves and will be used to estimate the δt. (d) result of the cross-correlation result (the lag corresponding to the maximum cross correlation coefficient is used to estimate the δt).

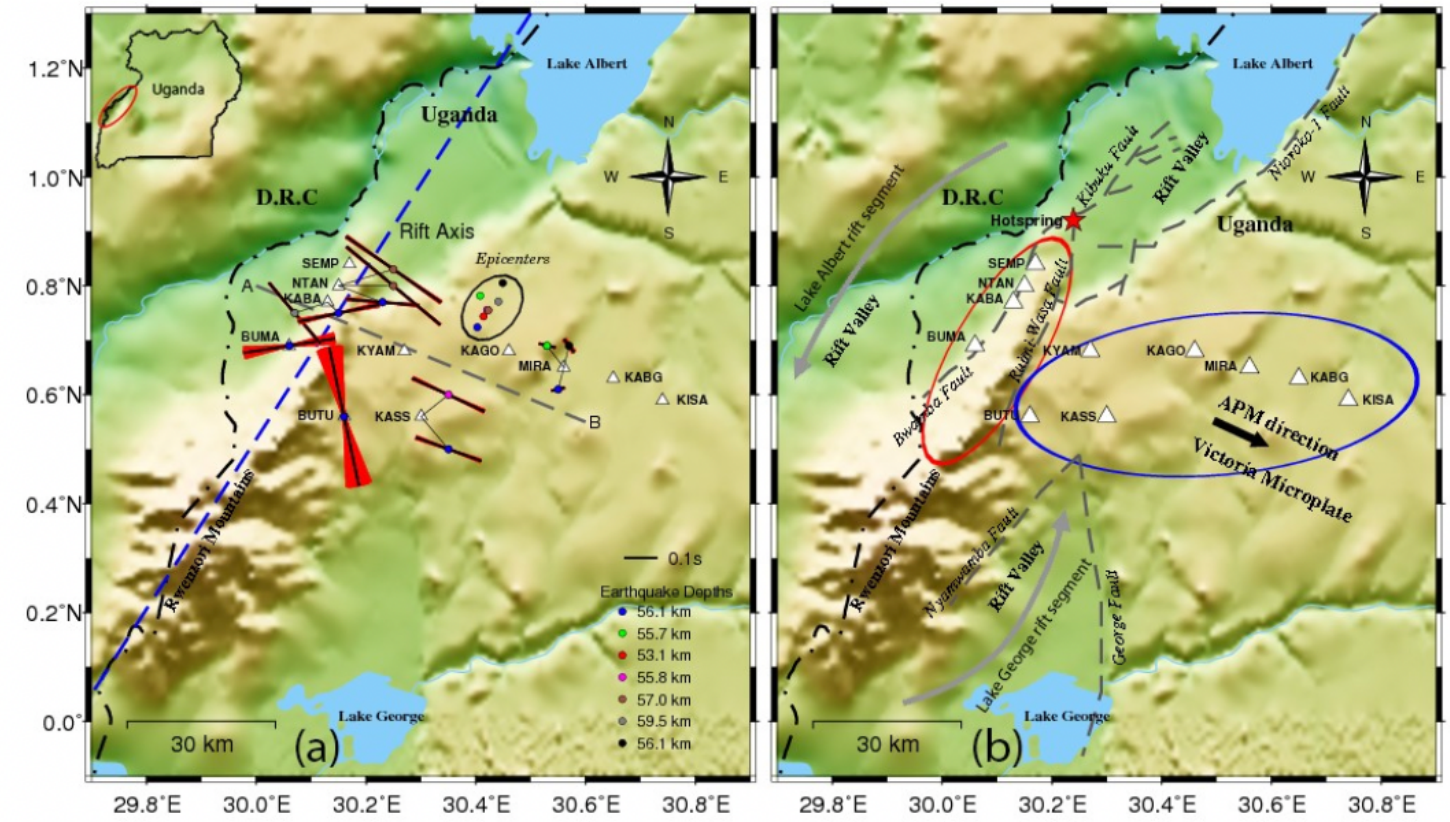

Figure 2

(a) Plot showing SWS results of the deep local earthquakes observed in the Rwenzori region. The splitting parameters are shown by the black bars, aligned by φ and scaled by δt. The red cones in the background represent the uncertainties in the splitting results at 95% confidence level. The earthquake epicenters are highlighted by the black ellipse and color coded basing on their depths. The white triangles are the seismic stations. The corresponding earthquake is plotted in the middle of each splitting parameter. The splitting parameters are projected onto profile A-B (gray dotted line) resulting into Figs 3a and 3b. (b) Showing the structural map of the region. The red and blue ellipses are demarcating the stations deployed in and outside the rift valley respectively.

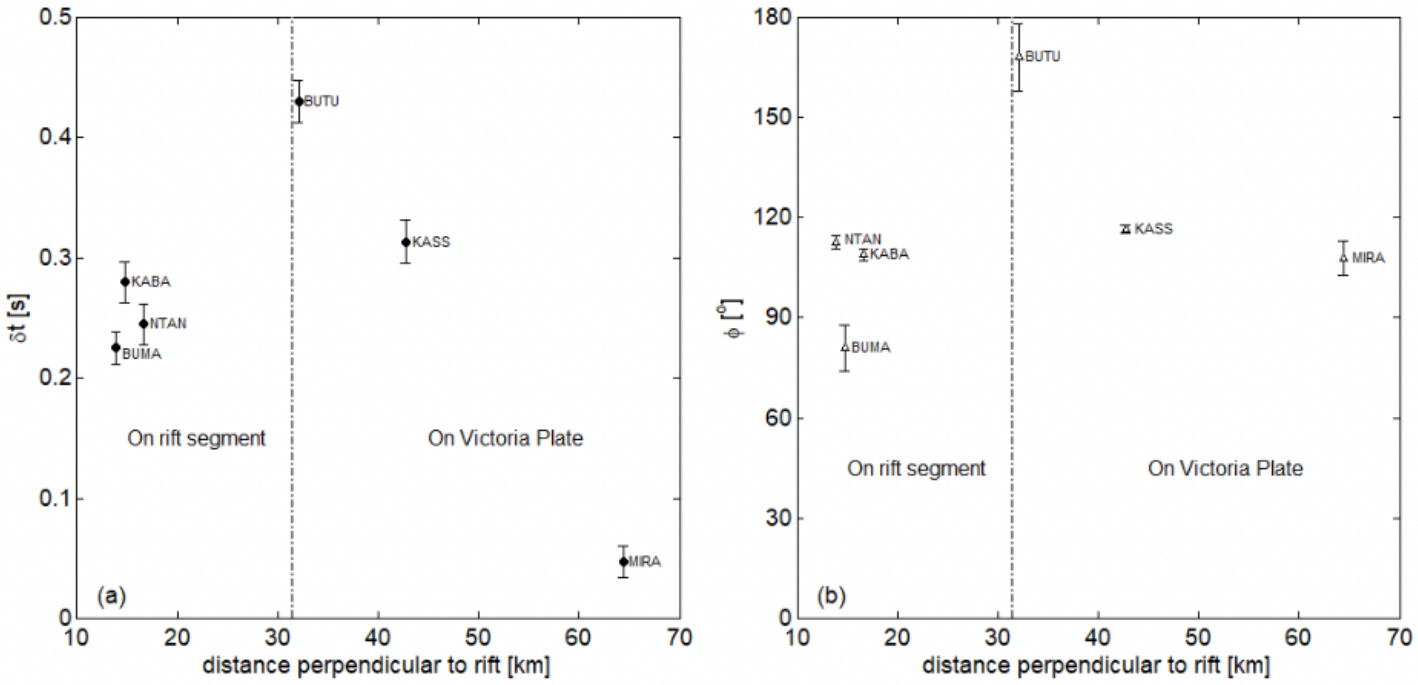

Figure 3

(a) Plot of average δt values against distance along profile A-B shown in Fig. 2a. (b) Plot of average φ against distance along profile A-B shown in Fig. 2a.

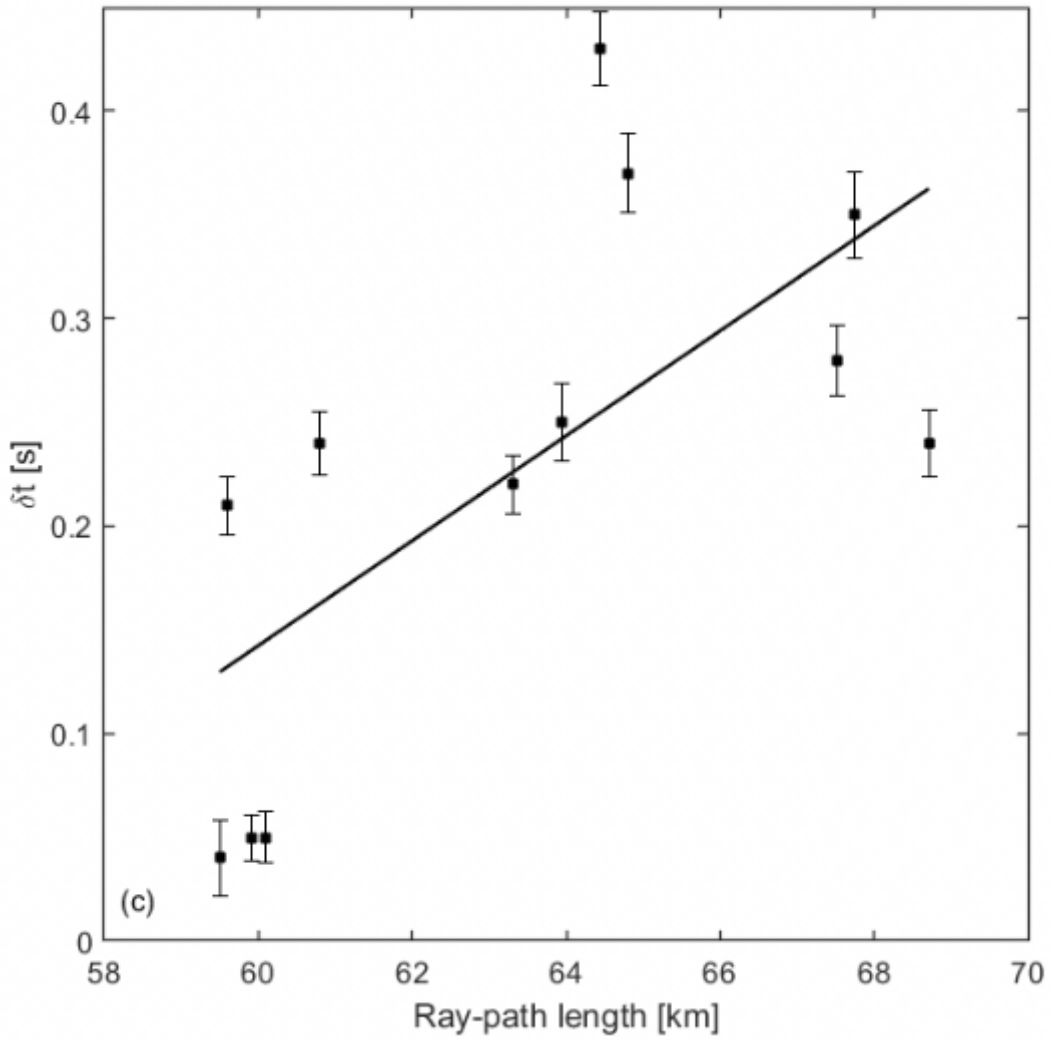

Figure 4

Plot of average δt values against ray-path length.

Supplementary Files

This is a list of supplementary files associated with this preprint. Click to download.

- Graphicalabstract.eps